Efficiently Compressing 3D Medical Images for Teleinterventions via CNNs and Anisotropic Diffusion

Ha Manh Luu
AVITECH & FET, University of Engineering and Technology, VNU, Hanoi, Vietnam
Department of Radiology and Nuclear Medicine, Erasmus MC, Rotterdam, the Netherlands

Theo van Walsum
Department of Radiology and Nuclear Medicine, Erasmus MC, Rotterdam, the Netherlands

Daniel Franklin
School of Electrical and Data Engineering, University of Technology Sydney, Sydney, Australia

Phuong Cam Pham
Nuclear Medicine and Oncology Center, Bach Mai Hospital, Hanoi, Vietnam

Luu Dang Vu
Radiology Center, Bach Mai Hospital, Hanoi, Vietnam

Adriaan Moelker
Department of Radiology and Nuclear Medicine, Erasmus MC, Rotterdam, the Netherlands

Marius Staring
Department of Radiology, Leiden University Medical Center, Leiden, the Netherlands

Xiem HoangVan
FET, University of Engineering and Technology, VNU, Hanoi, Vietnam

Wiro Niessen
Department of Radiology and Nuclear Medicine, Erasmus MC, Rotterdam, the Netherlands

Nguyen Linh Trung
AVITECH, University of Engineering and Technology, VNU, Hanoi, Vietnam

Version typeset January 27, 2021

Corresponding author. E-mail: halm@vnu.edu.vn

Abstract

Purpose: Efficient compression of images while preserving image quality has the potential to be a major enabler of effective remote clinical diagnosis and treatment, since poor Internet connection conditions are often the primary constraint in such services. This paper presents a framework for organ-specific image compression for teleinterventions based on a deep learning approach and anisotropic diffusion filter.

Methods: The proposed method, DLAD, uses a CNN architecture to extract a probability map for the organ of interest; this probability map guides an anisotropic diffusion filter that smooths the image except at the location of the organ of interest. Subsequently, a compression method, such as BZ2 and HEVC-visually lossless, is applied to compress the image. We demonstrate the proposed method on 3D CT images acquired for radio frequency ablation (RFA) of liver lesions. We quantitatively evaluate the proposed method on 151 CT images using peak-signal-to-noise ratio ($PSNR$), structural similarity ($SSIM$) and compression ratio (CR) metrics. Finally, we compare the assessments of two radiologists on the liver lesion detection and the liver lesion center annotation using 33 sets of the original images and the compressed images.

Results: The results show that the method can significantly improve CR of most well-known compression methods. DLAD combined with HEVC-visually lossless achieves the highest average CR of 6.45, which is 36% higher than that of the original HEVC and outperforms other state-of-the-art lossless medical image compression methods. The means of $PSNR$ and $SSIM$ are 70 dB and 0.95, respectively. In addition, the compression effects do not statistically significantly affect the assessments of the radiologists on the liver lesion detection and the lesion center annotation.

Conclusions: We thus conclude that the method has a high potential to be applied in teleintervention applications.

Contents

I. INTRODUCTION

Teleradiology is the transmission of the medical images such as CT, MRI, X-ray and Ultrasound over the Internet from one location to another for diagnostic or therapeutic decision-making. Teleradiology is becoming an increasingly important part of modern diagnostic medicine, although the capabilities of medical imaging technology continue to improve rapidly, the education of radiologists with the expertise required to fully utilize its capabilities has been unable to keep up. This has resulted in a lack of radiological experts, particularly in undeveloped/rural medical centers. At the same time, the rapid enrollment of the Internet worldwide has enabled increasingly convenient transfer of data among medical centers[1]. It has been reported that 86% of the radiologists in the United States have undertaken medical practice using teleradiology[2] while in an online survey, 74% of European radiologists claimed that teleradiology is currently used in their countries[3,4]. Teleradiology is now being employed in several developing countries in Africa, South America and Asia[5]. Vietnam has launched a teleradiology system which connected several hospitals during the Covid-19 pandemic in 2020[6].

Next to supporting radiological diagnosis, teleradiology has been used in the context of interventional therapeutic. Live teleinterventions in vascular endotherapy have recently been used for training of interventionalists via the Internet[7]. The interventions were often performed under the guidance of 2D angiography at a frame rate of 1-2 frame/s[8]. Teleultrasound scanning using 2D real-time US images has become popular in several telehealth applications[9]. However, live teleinterventions using 3D image modalities, such as CT-guided radiofrequency ablation (RFA) liver intervention is still challenging due to the frequently insufficient bandwidth for transmission of 3D CT images during live intervention. For example, a typical 3D CT image of 100 MB takes 5 to 8 minutes to be transferred between two locations via a network with an effective transmission speed of 2 Mbps, while a compressed image with a compression ratio of 6:1 may be transmitted within a minute. For some CT-guided liver interventions, such as tumor ablations, such a long waiting time is a significant delay in the procedure, compared to the average ablation time of 16 minutes (range 6-29 minutes)[10] while the delay is expected to be less than the scanning time (from few seconds to a minute). During the scanning time, the interventionists move out of the intervention room to avoid radiation expose and go back the intervention room after a brief overview of the acquired image.

Though modern broadband telecommunications technologies, such as 5G or optical fibers, are able to transmit with a speed of up to several Gbps, and with very low latency[11], this advanced infrastructure is not available in many regions. The 4G network has been shown to be able to transfer data from a hospital to other sites at a distance of 10 km and at a data rate up to 12 Mbps, however the package loss due to the unstable wireless channel is a challenge for live intervention application[11]. Coaxial cable seems to be a reasonable network for teleradiology, which enables to transfer data at a stable rate of 20-50 Mbps[12]. Another problem is that the networks are often a shared resource and the actual data transfer speed are much smaller than the maximum capability of the networks. In most hospitals and medical centers, LAN and WAN are available infrastructures which supply a typical data transmission rate of 10-100 Mbps, while the actual speed of a Wifi, under IEEE 802.11 standard, often are 2-5 Mbps[13]. Such regions with relatively poor Internet connectivity, therefore, are severely limited in their ability to take advantage of teleradiology, especially in live-view radiological interventions/operations. Image compression may enable effective utilization of teleradiology in such regions.

Several studies on methods for medical image compression have been published. These approaches fall into one of three categories: lossless, lossy or ROI-based compression methods. Lossless compression methods are often utilized because there is no reduction in image quality relative to the original. The compression ratios of various lossless compression methods (e.g. JPEG-LS, JPEG-2000, TIFF, PNG, CALIC, LZW, LZ77, and Gzip) range from 1.7 to 3.9 (Culnie, 2000)[14]. The original JPEG standard included a lossless compression option based on a simple differential PCM predictive coding scheme plus entropy encoding, while the more recent JPEG-LS employs a coding method based on a combination of separate decorrelation, error modelling and encoding schemes, which yields higher compression ratios and with lower computational complexity compared to the original JPEG lossless process[15]. HEVC also has a lossless option which has been used for medical image compression[16]. Beyond these general-purpose image compression standards, Mahenswari and Raghavan (2020) developed the tetrolet transform for medical image compression[17]. Amri et al. (2016) proposed watermark reduction combined with the standard JPEG-LS and TIFF formats[18]. Guarda el al. (2017) proposed a method to improve HEVC coding for volumetric medical image compression using Least-Squares Prediction (LSP)[19]. Lucas et al. (2016) proposed a method utilizing 3D predictors[20]. Hulsken (2020)[21] introduced a lossless wavelet-based method, iSyntax, to compress several types of medical images for web view purpose. In general, the main drawback of lossless compression methods is the low compression ratio and thus without further improvement, they seem to be not suitable for the live teleintervention application.

In contrast, lossy and near lossless compression methods offer much better compression ratios. Marcelo et al. (2000)[22] investigated standard lossy compression (JPEG) and reported that compressed (JPEG) images could be used for diagnosis with similar accuracy to using non-compressed images. Parikh et al. (2017) applied lossy HEVC for medical image compression, and determined a medically acceptable compression range for HEVC[23]. Sharma et al. (2019) proposed a detector (RIGED) and block adaptive arithmetic encoding (BAAE) for medical images[24]. The optimal level of quantization was selected based on overall visual quality as assessed by radiologists. Zerva et al. (2020)[25] introduced the 3D-WDR-MCPD method for lossily compressing 3D medical images, which explores the spatiotemporal coherence property to improve the compression ratio. Senapati et al. (2016)[26] proposed the 3D-HLCK embedded coder with the aim to reduce memory use in medical image compression. However, the use of lossy compression in teleradiology is still controversial because the reduced image quality may affect clinical decision-making.

In medical images, the regions of the image that contain information on the pathology, and that are being used for decision-making, are called regions of interests (ROIs); anything outside of these areas - the rest of the image - are denoted non-ROIs. The non-ROIs generally constitute the majority of the image. Therefore, ROI-based methods often losslessly compress the ROIs while lossily compressing the area outside the ROIs. Many researchers therefore define ROIs in the image and use a ROI-based method for achieving high compression ratios. In general, there are two strategies to define the ROIs. The first uses classical image processing methods such as such as graph cuts[27], region growing[28], levelsets and active shape/appearance models[29]; and the second utilizes modern machine-learning approaches, which can automatically separate ROIs with high accuracy and fast processing time. Recently, the machine learning approach has demonstrated superior performance over classical methods if a sufficient amount of training data is available[30]. Ahmadi et al. (2018)[31] used a CNN for segmenting ROIs and background from an angiogram image. A DCT was used for tilling the ROIs and non-ROIs, after which the image was smoothed via Gaussian blurring, followed by JPEG-LS-based compression. Wavelet transforms were also used to lossily compress the non-ROIs[32,33,34,35]. Sreenivasulu and Varadarajan (2018) applied a DCT and hierarchical tree encoding method for ROI compression[28]. Manpreet and Wassona (2015) processed the ROIs by context tree weighting, and applied fractal lossy compression for the non-ROIs[36]. Other approaches applied lossy compression methods for both the ROIs and the non-ROIs with different quality. Kurma et al. (2018) introduced the CVQ-SA method which compresses the ROIs with a low compression ratio and the non-ROIs with a high compression ratio[37]. Chaabouni et al. (2016) first applied a DWT, and then compressed the coefficients using an incremental self organizing map (ISOM)[27]. However, those methods do not preserve the edges in non-ROIs, which may be relevant in separating the objects in medical images.

The main challenges of medical image compression methods for live interventions are:

1. The compression rate should be sufficiently high while preserving the image quality for clinical purposes (should be larger than 6); and
2. The compression and decompression process must be sufficiently fast (should be in order of seconds).

In this paper, we propose an image processing method, deep learning and anisotropic diffusion (DLAD), to improve medical image compression for live interventions using 3D images. Our approach falls under the ROI compression approach. The proposed method exploits the principle of Shannon's information theory[38] that the smoothed version of an image contains less entropy than the original image. Therefore, compressing the smoothed image should achieve higher compression rates compared to the original image. Our approach is to first apply a trained application-specific convolutional neural network (CNN) to the image for extracting a probability map, which highlights the organ of interest region. Subsequently, the probability map modulates the diffusion coefficient function of an anisotropic diffusion filter, which controls the rate of diffusion in the original image. Differing from the other lossy ROI-based compression methods, the key idea of our method is that the anisotropic diffusion filter blurs the homogeneous areas outside the organ of interest region while preserving the edges and keeping the organ of interest region undiffused. Finally, the diffused image is compressed using a conventional compression method.

We demonstrate the proposed compression framework for liver RFA interventions using CT images. During the intervention, the interventionist performs tumor ablation under CT guidance[39] (see Figure 1). With single-ablator interventions, one of the key factors for the success is that the tip of the ablator needs to be positioned at the center of the tumor[40]. Therefore, locating the tumor centers in the CT images is a critically important task for the radiologist/interventionist.

Figure 1: A CT-guided along with US-guided intervention of the liver RFA ablation[41].

To perform the image compression, the probability map is derived from the interventional CT image utilizing a fully convolutional network (FCN) based on the well-known U-net architecture[42,43]. The probability map is then embedded in the diffusion coefficient function of a Perona-Malik diffusion filter[44]. Afterwards, a lossless compression method (such as BZ2)[45] visually lossless method (such as HEVC)[46], is applied on the diffused image. In our study, we assess the extent to which image compression artifacts affect the radiologist's assessment of the liver intervention images. This is crucial because image compression artifacts should not affect the diagnostic assessment and treatment quality. In this study, two radiologists perform the liver lesion detection and the liver lesion center localization. Based on the score of their assessments, compared with the ground truth, we qualitatively evaluate the effect of the image compression on the clinical process.

The remainder of the paper is organized as follows. The next section presents the compression process, the proposed image processing method based on CNN and diffusion filter, as well as the two conventional image compression methods. In Section III., we describe the experiments and evaluation of the proposed method which includes image quality metrics and assessments by radiologists. Section IV. discusses the implications of these results, while the final section summarizes the outcomes and draws conclusions from the study.

II. METHOD

II.A. CNN-based liver probability map extraction

In this study, we applied a fully convolutional network (FCN) based on the well-known U-net architecture[47] to extract the probability map $P(I(\mathbf{x}_i)) = \{p(\mathbf{x}_i)\}$ of the liver CT image I, where $\mathbf{x}_i$ is the position of the i-th voxel[42]. The probability $p(\mathbf{x}_i) \in [0, 1]$ should yield the value of closing to 1 when $\mathbf{x}_i$ is inside the liver region while approaching 0 outside of the liver region. The FCN network introduced by Christ et al. (2017)[42] was used to compute the probability map of the each 2D slice of the 3D interventional CT image. The key idea of a FCN is that it contains only convolutional layers, which allows the last layer of the network to predict dense pixel-wise probabilities for an image. The FCN contains 19 layers, which are organized in five stages of the U-net architecture (see Figure 2). We chose the FCN model due to its intrinsic multiscale structure and the good results reported in other related applications. The relatively small size of the network allows the probability map to be extracted within a short computation time. As in the experiments in our previous study[43,48], the computational time, using a modern GPU, for the whole 3D liver CT image is few seconds, while the inference time for a single 2D slice is of the order of several hundred milliseconds on average.

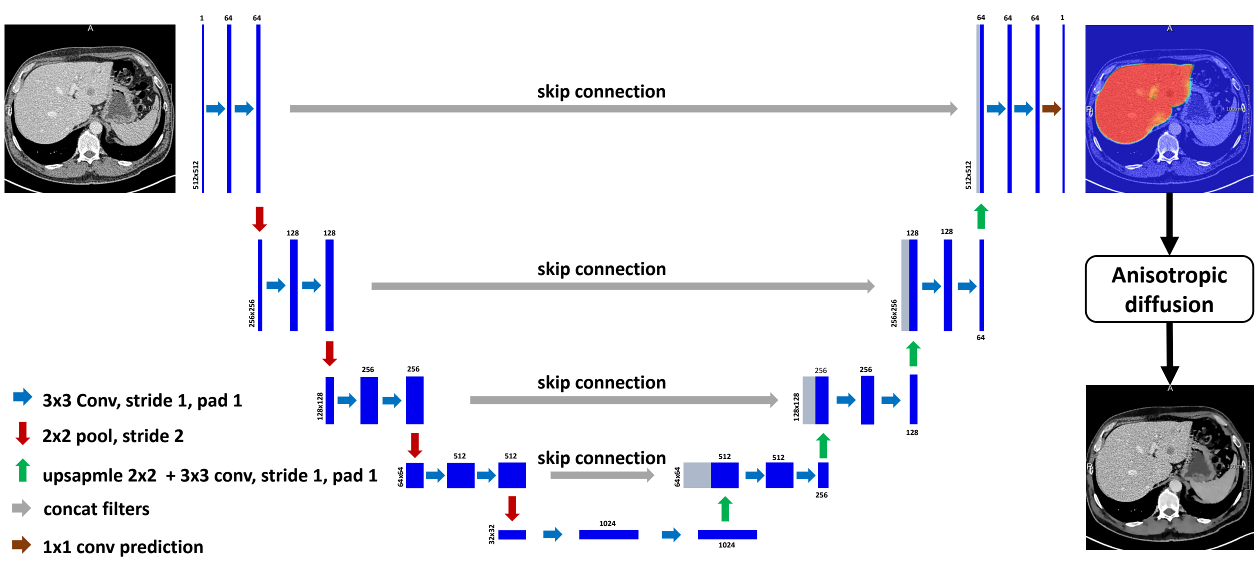

Figure 2: The proposed DLAD method: A 2D U-net architecture processes the 2D CT images and outputs 2D liver probability maps. These maps are used to steer the anisotropic diffusion filter. The FCN network contains five levels in a hierarchical structure.

II.B. Deep learning anisotropic diffusion filter

Based on the fact that entropy coding can be used to compress the image[49], our strategy for improving the compression rate is to reduce the entropy of the image[38] by applying an anisotropic diffusion process on the images. It already has been demonstrated that a blurred version of an image has smaller entropy than the original image[50]. In this section, we describe the anisotropic diffusion filter used in this work. The filter has two important properties:

1. It does not diffuse inside the liver region; and

2. It diffuses less at the edges while diffusing more in homogeneous regions.

The diffusion process of the image *I* can be described as the following equation[44]:

$$\frac{\partial I(\mathbf{x}_i, t)}{\partial t} = div(C(\mathbf{x}_i, t)\nabla I) = \nabla C(\mathbf{x}_i, t)\nabla I + C(\mathbf{x}_i, t)\triangle I, \tag{1}$$

where ∇ is gradient operator, $\triangle$ is Laplacian operator, *div(...)* is divergence operator and $C(\mathbf{x}_i, t)$ is a diffusion coefficient function. In this study, we proposed the following diffusion coefficient function:

$$C(\|\nabla I(\mathbf{x}_i)\|, p(\mathbf{x}_i)) = (1 - p(\mathbf{x}_i))exp(-\frac{\|\nabla I(\mathbf{x}_i)\|}{K}), \tag{2}$$

where $\|\nabla I(\mathbf{x}_i)\|$ is the magnitude gradient of the image *I*, $p(\mathbf{x}_i)$ is the probability values of the probability map $P(I(\mathbf{x}_i))$ and K is conductivity parameter which rescales gradient magnitude values. This diffusion coefficient function ensures that when $p(\mathbf{x}_i) \rightarrow 1$, the function $C(\|\nabla I(\mathbf{x}_i)\|) \rightarrow 0$, i.e. there is no diffusion in the liver region, while when $p(\mathbf{x}_i) \rightarrow 0$, $C(\|\nabla I(\mathbf{x}_i)\|)$ depends more on the value of the magnitude gradient image $\|\nabla I(\mathbf{x}_i)\|$ (at a specific time point t).

II.C. Image compression methods

The aim of the proposed method is to reduce the entropy of the image to achieve a higher compression rate for several well-known compression methods. Furthermore, we intend to use lossless compression methods because they do not affect the quality of the images, which is relevant for medical applications. For the live intervention application, the compression methods should allow fast decompression because typically the receiver devices have low computational power while the computational power of the transmitter can easily be matched by advanced hardware (such as a computational cluster or modern GPUs). Therefore, image compression methods which require long decompression times, such as JPEG-LS and JPEG2000, are not suitable for our application. In this section, we briefly present two compression methods, BZ2 and HEVC, which support lossless and visually lossless compression, respectively. Those methods will be assessed in the experimental section and then compared to several well-known lossless compression methods such as Gzip (GZ), Rar (RAR), Zip (ZIP), 7Z, JPEG-LS (JLS), JPEG2000 (J2K), iSyntax[21] and Set partitioning in hierarchical trees (SPIHT)[51].

BZ2, also called Bzip2, is a lossless compression algorithm mainly based on the Burrows–Wheeler transform (BWT)[52] and Huffman coding[53]. BWT is block-sorting text compression algorithm, which rearranges a symbol string into runs of similar symbols[54]. The rearranged symbols are then effectively compressed by applying Huffman coding. The 3D CT images can be considered as a raw data stream and thus can be compressed using BZ2. In addition, Patel et al. (2012) suggested that BZ2 can be implemented in parallel in multicore CPUs and GPUs to reduce processing time[55].

HEVC, also called H.265, is a state-of-the-art compression standard which can be used for both video and image compression[56]. HEVC achieves a high compression ratio because it contains several advanced techniques such as spatial and temporal prediction, DST and DCT transforms, quantization and entropy coding[23]. HEVC-lossless/visually lossless compressions[46] are suitable for medical image compression[16,19,23,57,58]. Furthermore, HEVC also can be implemented in parallel and thus also can potentially be applied in live teleinterventions[59].

III. EXPERIMENT AND EVALUATIONS

III.A. Dataset and annotations

We used 151 abdominal diagnostic and interventional CT images aquired before and during RFA liver interventions, which were retrospectively used in our previous studies[43,60]. The datasets were collected from three sources: Erasmus MC, Mayo Clinic and LiTS challenge. The images were acquired on Siemens, GE and Philips scanners and were reconstructed according to standard medical protocols. All datasets were anonymized before they were used in this study. The images were converted into $nifti$ format with 16-bit depth. The details of the datasets are

Table 1: Characteristics of the datasets used in this study.

Dataset	Number of images	In-plain resolution (mm)	Spacing (mm)	Number of slices	Voltage (kV)	Tube current (mAs)
EMC	103	0.55-0.98	0.8-10.0	21-261	80-120	4-12
Mayo	20	0.66-0.82	3.0	128-343	100-120	18-21
LiTS	28	0.63-1.0	0.7-5.0	31-234	-	-

summarized in Table 1. Of those datasets, 33 contrast-enhanced CT images with 61 visible liver legions (35 HCCs, 20 metastases, 3 benign cysts and 3 hemangiomas), 1 to 5 lesions per image with diameters smaller than 3 cm, were selected for the radiologist evaluation section. The selected images contain either liver tumor segmentations or tumor center markers performed by a certified radiologist and then reviewed by one to three radiologist experts. From the liver tumor segmentations, we determined the center of the tumors by extracting the middle point of the longest diameter of the tumor segmentations. Those centers were used as the ground truth in the radiologist evaluation section (Section III.D.1.). Table 1 lists the characteristics of the datasets used in this study.

III.B. Quantitative evaluation criteria

III.B.1. PSNR

$PSNR$ is commonly used to measure the quality of lossy image compression method. $PSNR$ is defined as the ratio between the maximum possible power of a signal and the power of the difference between in intensities of the original image and the reconstructed-compressed image (the diffused image). Generally, $PSNR$ for a 3D image is formulated as follows:

$$PSNR = 10 \log_{10}(\frac{L^2}{MSE}), \tag{3}$$

$$MSE = \frac{\sum[I(x_i) - D(x_i)]^2}{V}, \tag{4}$$

where $L = 2^{16} - 1$ for 16 bit depth CT images, MSE is the the average power of the difference of the the original image $I(\mathbf{x}_i)$ and the compressed image $D(\mathbf{x}_i)$ across a total of V voxels.

III.B.2. SSIM

While $PSNR$ quantifies the difference of the two images globally, $SSIM$, introduced by Wang and Bovik (2004)[61], measures the quality of the image based on the fact that the pixels/voxels have a strong relation when they are spatially close. The SSIM index of two images is calculated using the following formula[62]:

$$SSIM(x,y) = \frac{(2\mu_x\mu_y + C_1)(2\sigma_{xy} + C_2)}{(\mu_x^2 + \mu_y^2 + C_1)(\sigma_x^2 + \sigma_y^2 + C_1)}, \tag{5}$$

where x and y are pairs of local square patches at the same spatial locations (as sub-volumes/sub-images of image I and D respectively); μ_x and μ_y are the mean intensity values of the two corresponding patches x and y; σ_x and σ_y are standard deviations of the intensities of the patches x and y respectively; σ_{xy} is the covariance intensities of the of the two patches; $C_1 = (K_1L)^2$ and $C_2 = (K_2L)^2$, with K_1 and K_2 are preset constants, are variables to stabilize the division by the small dominator. In this study, we chose $K_1 = 0.01$ and $K_2 = 0.03$ and the patch size of 11x11x1 with Gaussian weight scale of $\sigma = 1.5$ as suggested by Nilsson (2020)[63].

III.B.3. Compression ratio

The compression ratio, CR, measures the ratio between the original image size and the compressed image size:

$$CR = \frac{OS}{CS}, \tag{6}$$

where OS and CS are the original image size and the compressed image size, respectively.

III.B.4. Radiologist assessments

$PSNR$ and $SSIM$ are objective image quality metrics that are not explicitly related to diagnostic and treatment decision-making by medical experts. In this study, two radiologists, with 3 and 8 years of experience in reading liver tumors and performing RFA liver intervention using CT images, detected the liver lesions and annotated the centers in the CT images. Specifically, the 33 CT images, with the ground truth of the liver lesion centers (section III.A.), were processed using the proposed DLAD method and then compressed using BZ2 and HECV-visually lossless method. The file names of the original and decompressed images were anonymized and sorted in a random order. The two radiologists blindly read and annotated the center of the detected lesions in each image separately. In addition, the spatial accuracy of the liver tumor center annotation is important because the radiologist typically aims to insert the RF ablator through the center of a tumor in liver RFA interventions. Therefore, for the TP detection annotations, we compute the

Euclidean distances between the liver lesion annotations by the two radiologists and the ground truth.

For the liver lesions detection evaluation metric, we used a per-lesion scoring metric as suggested by McCollough (2017)[64] as follows:

- The reader gets +1 point for a true positive (TP) lesion detected, i.e. when the annotated center is less than 10 mm apart;
- The reader gets -1 point for a false positive (FP) lesion annotation;
- The reader gets -1 point for a false negative (FN) lesion annotation;
- The normalized score (NS) is the total score/number of lesions (expressed as a percentage); and
- The sensitivity score (SC) is TP/(TP+FN) (expressed as a percentage).

Note that the evaluation does not include true negative (TN) score because it is medically necessary to detect the liver tumor rather than the healthy liver parenchyma in the RFA intervention.

III.C. Implementation and parameter verification

The study was carried on an Ubuntu 16.04 Linux PC, with a 2.40 GHz 16-core Intel® E5-2665 Xeon® CPU, 64 GB DDR3 and 1333 MHz bus. The proposed DLAD method was implemented using the ITK 5.1.1 library in C++ with a Python 3.7 wrapper. The CNN model for the liver probability map extraction was reused from our previous study[43], which was trained on 115 CT images from the LiTS dataset[65] using an NVidia TITAN V GPU and was tested on 40 contrast enhanced CT images of the liver. The parameter settings for training the CNN model were inhered from the the original work by Christ et al. (2017)[42]. In this study, the probability map is dilated with a circular kernel of 30x30x1 voxels and then is thresholded so that the probability values are 1 when they are larger than 0.75 to ensure the liver is inside the undiffused region. As investigated in our previous study[43] that the threshold of 0.75 guarantees liver segmentation from the probability map to be larger than 90 % on average.

Compression and decompression were performed with Python 3.7 using only the CPU. We used BZ2 compression which is available as a standard Linux library and standalone utility. HEVC-visually lossless, implemented in the *FFMPEG* library in multicore CPU, was applied to compress each 2D slice of the image (the implementation has no support for 3D image compression yet). $PNSR$ and $SSIM$ scores were computed using the *Skimage* library while the entropy of the image was measured using the *Scipy* library. ISyntax source code was implemented and experimented in Matlab 2018b, provided by the author[21].

In the parameter tuning section for the DLAD method, we use the 10 images in the Mayo dataset as a training dataset. We performed the diffusion while varying the number of iterations and the conductivity parameter K. The results of the experiment are shown in Figure 3. While the $PSNR$ score does not show differences w.r.t the number of iterations (Figure 3a), the $SSIM$ and CR score are both strongly dependent on these two parameters. According to Flynn (2013)[66], the processed image should maintain an $SSIM$ score higher than 0.95 to ensure visual acceptance. In addition, the number of iterations should be as low as possible to limit the processing time. Note that the number of iterations is linearly related to the processing time while the compression ratio does not linearly increase with the number of iterations. Thus, we chose the optimal conductivity parameter $K = 0.4$ and the number of iterations as 15. A summary of the pilot experiment using the BZ2 compression method is provided in Table 2.

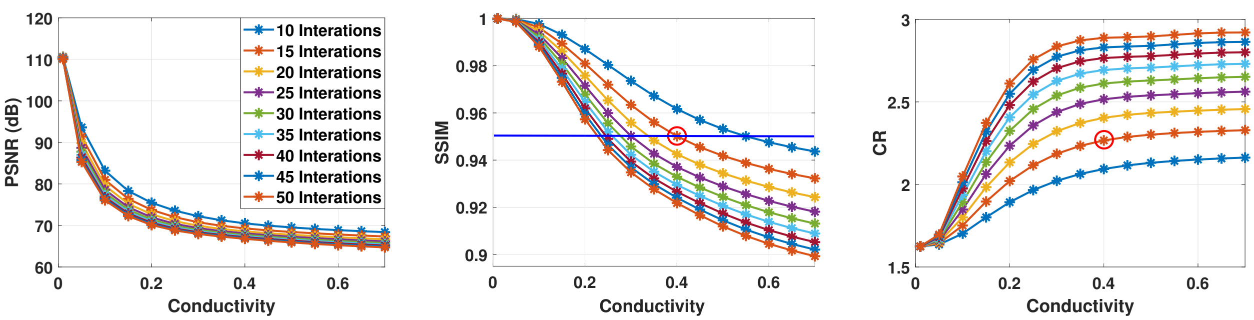

(a) Peak signal-to-noise ratio (b) Structural similarity (c) Compression ratio

Figure 3: The effect of varying the number of iterations and the conductivity parameter K on the $PSNR$ score (a), $SSIM$ score (b) and the compression ratio (c) on average. The circle is at the optimal parameter point.

Figure 4 is an example CT image processed by the DLAD method. In the diffused image (B) the liver region is indistinguishable from the original (A), whereas the rest of the image is anisotropically diffused. Moreover, the histogram of the diffused image is more peaked than that of the original image, with a corresponding lower entropy value (8.72) than the original image

Table 2: The evaluation on the pilot images (Mayo) with the conductivity parameter $K = 0.4$ and the number of iterations = 15 using CPU only. The average entropy shows that the diffused images have lower entropy than that of the original images. The numbers in (parentheses) are the standard deviations while the numbers in the [square bracket] are the min and the max values. The compression ratio is for the BZ2 method.

Number of slices	**Diffusion time (s)**	*PSNR* **(dB)**	*SSIM*	*CR*	**Entropy**	
					Original	**Diffusion**
90.5 [75-110]	34.7 [32.4-36.8]	70.33 (0.85)	0.95 (0.02)	2.25 (0.20)	9.15 (0.12)	8.66 (0.20)

(9.14). The average entropy of the full set of diffused Mayo images (8.66) is also lower than the average entropy of the original images (9.15) (Table 2)

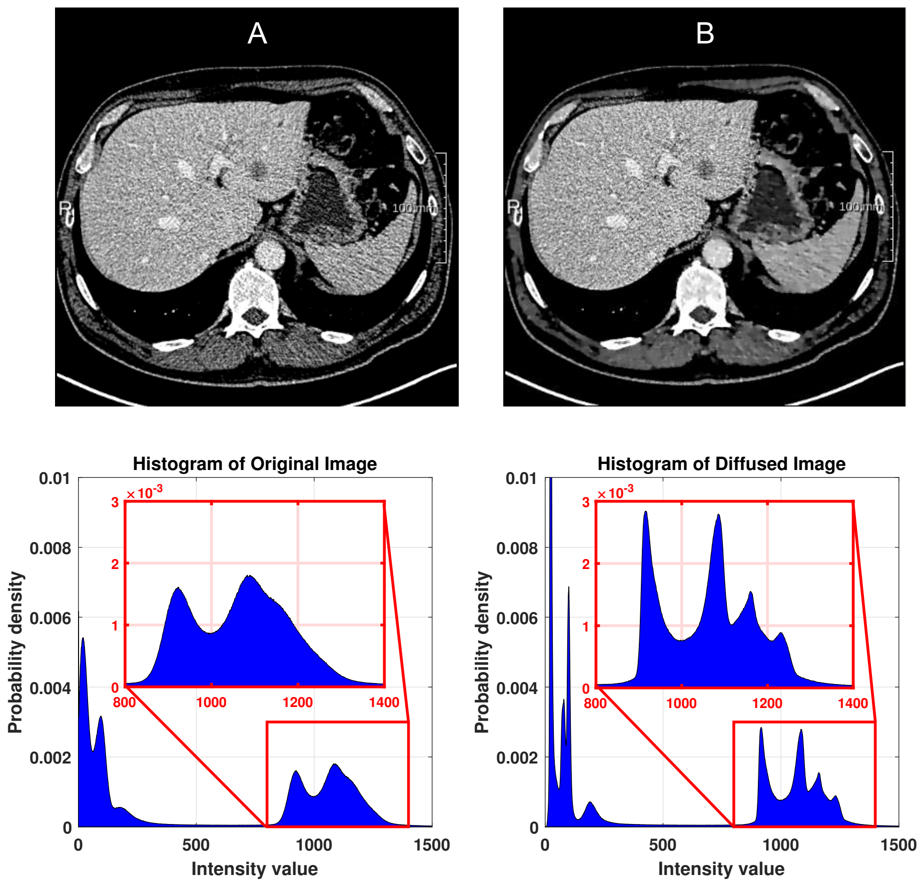

Figure 4: An example of the effect the DLAD method on a liver CT image: The original image (the left) and the diffused image (the right) have entropy values of 9.14 and 8.72, respectively.

III.D. Experiment results

III.D.1. Quantitative evaluation results

We applied the DLAD diffusion on the rest of the datasets (141 CT images). The diffused images were compressed with several well-known lossless compression methods such as GZ, RAR, ZIP, BZ2, 7Z, JLS, J2K, iSyntax, SPIHT and HEVC-visually lossless. The compression ratios of the original images and the diffused images are shown in Figure 5 and Table 3 for each of these compression methods. HEVC-visually lossless achieves the highest compression ratio, compressing the original images and the diffused images by factors of 4.73 and 6.45, respectively, with the improvement of 36%. We also perform paired T-tests on the compression ratios for the original images versus those of the diffused images. The results show that for all of the compression methods, the improvement in compression ratios with diffused vs. original images was statistically significant, with p-values of smaller than 0.01. The results also suggest that the HEVC compression method on the DLAD diffused image statistically significantly performed better than the other compression methods ($p < 0.001$).

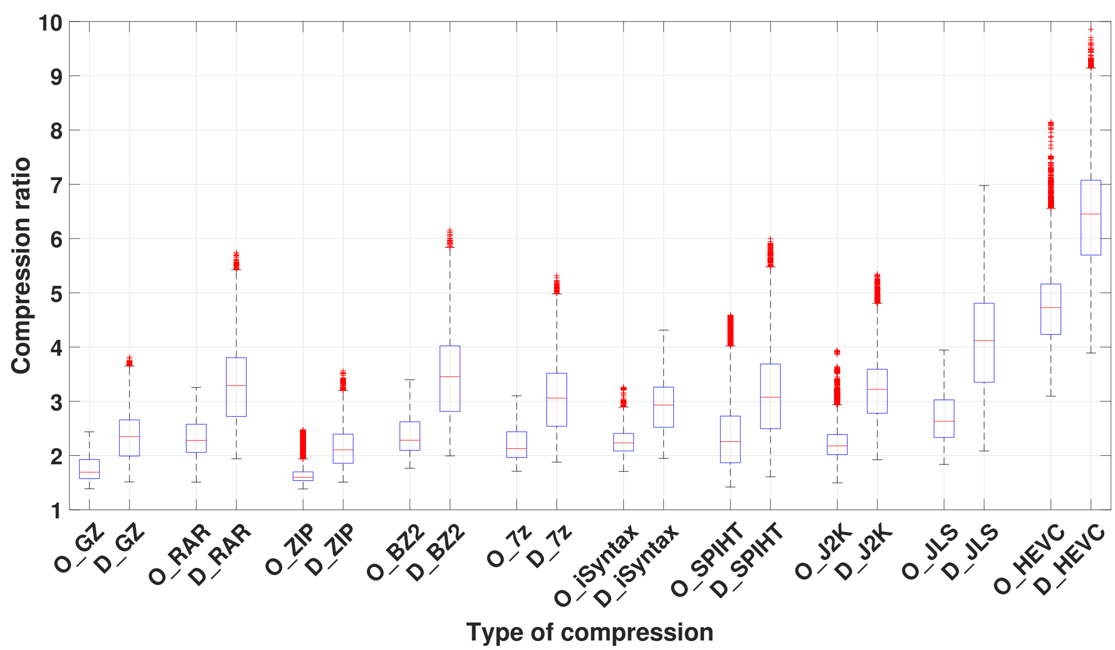

Figure 5: : The compression ratios achieved by each compression method on the original images (the left) and the DLAD diffused images (the right).

The average computation time of the compression methods on a 2D slice of the original images and the diffused images, using the CPU only, are shown in Figure 6. It can be seen that,

Table 3: Compression ratios, maximum processing time and maximum memory usage of several compression methods applied on the abdominal 3D CT images. The numbers in the round bracket are standard deviations. The implementation of iSyntax is in Matlab with unreliable computation time and used memory resource, and thus those values are not included in the table.

		Type of compression									
		GZ	**RAR**	**ZIP**	**BZ2**	**7z**	**iSyntax**	**SPIHT**	**JLS**	**J2K**	**HEVC**
Median of compression ratio	Original	1.7 (0.21)	2.28 (0.33)	1.6 (0.2)	2.28 (0.32)	2.13 (0.28)	2.26 (0.26)	2.54 (0.94)	2.63 (0.42)	2.18 (0.32)	4.73 (0.77)
	Diffusied	2.1 (0.37)	3.29 (0.70)	2.34 (0.43)	3.45 (0.78)	3.06 (0.63)	2.93 (0.51)	3.3 (1.07)	4.12 (0.95)	3.22 (0.61)	6.45 (1.06)
Improvement		33% (14%)	44% (18%)	29% (14%)	47% (20%)	38% (16%)	29% (15%)	33% (24%)	53% (22%)	46% (19%)	36% (13%)
Maximum processing time (s)		23.1 (18.4)	26.8 (22.3)	23.6 (19.9)	23.8 (19.0)	34.9 (28.6)	-	32.8 (21.3)	27.5 (22.6)	38.2 (34.0)	36.3 (29.4)
Maximum memory usage (MB)		490.7	490.8	491.2	499.6	597.0	-	490.9	490.9	490.9	490.9

in general, all of the compression methods require less than a half of a second to compress and decompress a single 2D liver CT image. In addition to the diffusion processing time and the liver probability map extraction time (using the CPU), the whole process requires an average processing time of less than one and a half minutes for a 3D CT image of 90 slices (see Table 2). Moreover, the J2K and JLS compression methods require more time to decompress than to compress the images.

Figure 7 illustrates the differences between the original image (A) and the images with BZ2 (B) and the HEVC (C) compression. The difference images show that the BZ2-compressed image does not show any difference in the liver region, since it is lossless in this region; the HEVC-compressed image yields some tiny differences in the liver region. The $PSNR$ and $SSIM$ score are computed within the liver region of the HEVC-decompressed diffused images, yielding average values of 92 dB and 0.998, respectively.

III.D.2. Radiologist assessment result

Liver lesion detection by the two radiologists on the images with BZ2 and the HEVC-compression is summarized in Table 4. The table shows that the sensitivity metrics for radiologist 1 and 2 to the original images are 67.2% and 72.1%, respectively. Those scores are within the range [53% - 81%] of the expected performance of radiologists in the task of liver lesion detection reported in Fletcher et al. (2018)[67]. Both radiologists detected one or two lesions fewer in the diffused images and the diffused HEVC images, which are not statistically significant ($< 5\%$).

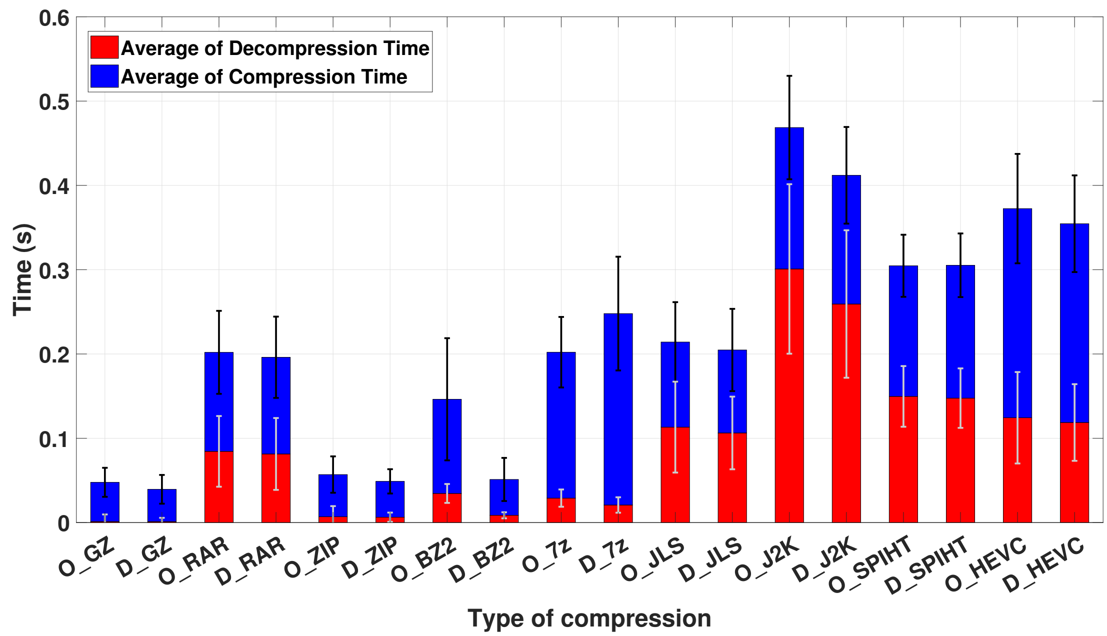

Figure 6: The average compression and decompression times of the different compression methods on both the original images and the diffused images. The prefix "O" indicates that the compression ratios are for the original images, while the prefix "D" indicates that the result is for the diffused images. The computation time of iSyntax is excluded due to the unreliable implementation for time-consuming measurement in Matlab.

Moreover, false detections are fewer in the decompressed images than that in the original images. The NS scores suggest that radiologist 2 (with 8 years of experience) performs better than the radiologist 1 (3 years of experience), but there is no significant difference in the performances of the two radiologists.

Figure 8 illustrates the displacements in the annotations at the liver lesion centers performed by two radiologists. The median values of the displacements for the original, BZ2-decompression diffused and HEVC-decompression diffused images by radiologists 1 and 2 (with the standard deviations in parentheses) are 2.4 (1.6) mm, 2.2 (2.2) mm, 2.6 (1.9) mm, 2.0 (1.3) mm, 2.3

Table 4: The evaluation scores performed by the two radiologists on the 33 sets of the original, the BZ2-decompression diffused and the HEVC-decompression diffused images.

Evaluation parameter	Radiologist 1			Radiologist 2		
	Original	Difffused-BZ2	Diffused-HEVC	Original	Difffused-BZ2	Diffused-HEVC
TP	41/61	39/61	40/61	44/61	43/61	42/61
FP	21	16	19	15	13	12
FN	20	22	21	17	18	19
SC (%)	67.2	63.9	65.5	72.1	70.4	68.8
NS (%)	0.0	1.6	0.0	19.7	19.7	18.0

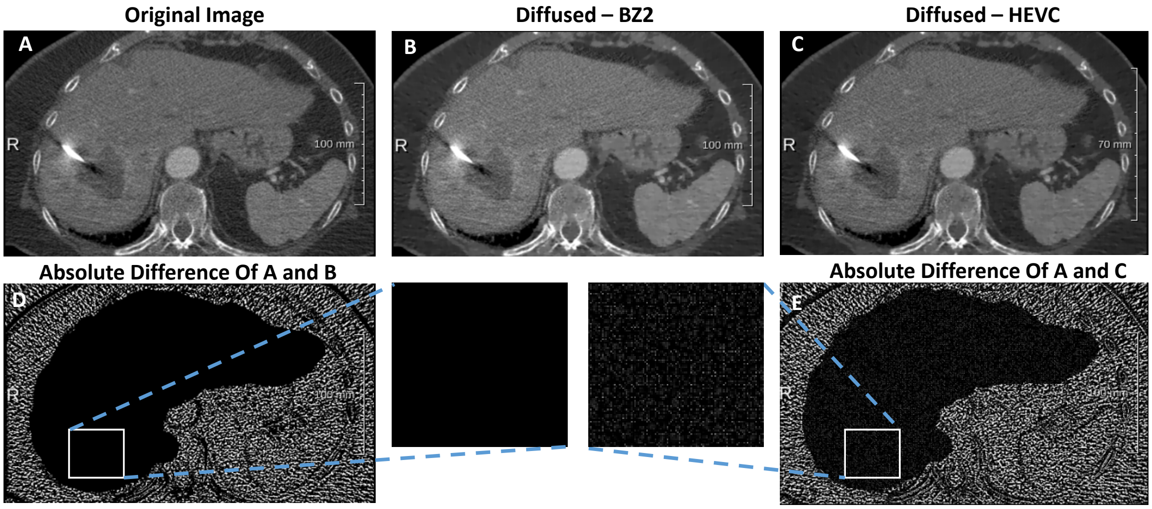

Figure 7: Examples of the decompressed CT images in RFA liver intervention using BZ2 and HEVC method.

(1.6) mm and 2.3 (1.3) mm, respectively. The p-values for T-tests on the performance of the radiologist 1 and 2 with "Original" vs "Diffused-BZ2", and "Original" vs "Diffused-HEVC" are 0.72, 0.25, 0.13 and 0.53, respectively. There are thus no statistically significant differences in placing the liver lesion centers when comparing the radiologists performance on the original images and the compressed images. The medians of the difference in placing the annotations between the two radiologists are 0.97 (2.76) mm, 1.08 (2.53) mm and 1.04 (2.38) mm, respectively. The p-values for T-tests on the inter-observer performance with "Original" vs "Diffused-BZ2", and "Original" vs "Diffused-HEVC" are 0.36 and 0.91, respectively, suggesting that there is no statistically significant difference in annotating the liver tumor centers by the two radiologists.

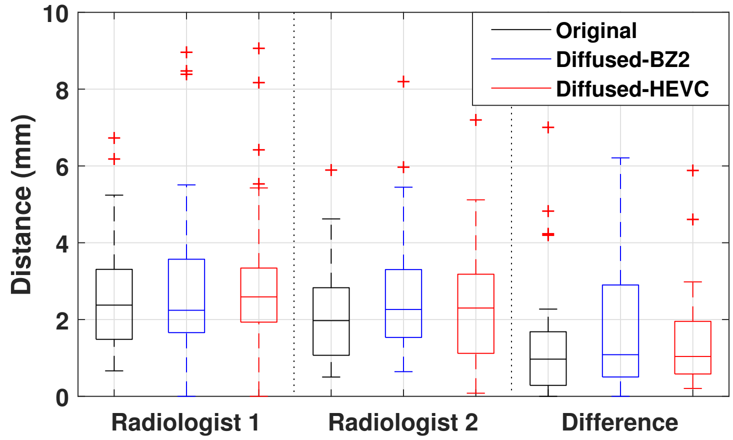

Figure 8: The distances between the annotations at the liver lesion centers performed by the two radiologists and the ground truth of the liver tumor centers. "Original" is the displacements in the original images, "Diffused-BZ2" indicates the displacements in the BZ2-decompression diffused images, while "Diffused-HEVC" stands for the displacements in the HEVC-decompression diffused images. "Difference" illustrates the distances between the annotations of the radiologist 1 and 2 at the same liver lesions.

IV. DISCUSSION

The experimental results presented in Section III.D.1. show that the JLS compression method achieves a median compression ratio of 4.12 (0.95) which is the highest compression ratio among the lossless compression methods, while HEVC-visually lossless achieves the highest median compression ratio of 6.45 (0.95). These results are comparable to those of the best state-of-the-art of medical image compression methods[17,19,20,23,28,37,58]. A summary of the state-of-the-art medical image compression methods is listed Table 5. The DLAD method is a preprocessing method to reduce entropy of the images while maintaining the quality of the image for medical purposes, and thus it may also be combined with other compression methods. Parikh et al. (2016) suggested that lossy HEVC-based compression can reduce the size of a medical image by up to 71-94%, and Pole and Shriam (2018) showed that the proposed lossy HEVC method for compressing 3D medical images achieves a CR of 10-15. Obviously, the lossy HEVC-based methods perform better than our proposed method; however, we suggest that the effect of the lossy compression methods should be carefully verified for the specific medical application by the (interventional) radiologists before being a compression scheme is chosen in practice. Recently, the H.266 compression method has been released[68]; it is expected that the combination of DLAD and H.266-lossless also has great potential in medical image compression applications.

Table 5: The summary of the state-of-the-art for 3D medical image compression methods.

Citations	Method	Data (3D)	*PSNR* (dB)	*SSIM*	*CR*	Max processing time (s)	
						Comp.	Decomp.
Kurmar *et al.* (2018)[37]	ROI lossy/ CVQ - SA	10 abdomen CT images	39.0 (1.0), [37.27 - 40.28]	-	6.27 (0)	-	-
Sreenivasulu *et al.* (2020)[28]	ROI lossless/ Wavelet	5 images (Brain MRI)	42.3 (3.3), [38.65 - 46.69]	-	2.6 (0.8), [1.68 - 3.88]	-	-
Lucas *et al.* (2017)[20]	Lossless/ 3D predictors	CT and MR image	-	-	4.1 (1.8), [2.57 - 8.38]	220148.7	15.1
Parikh *et al.* (2018)[23]	Lossy/ HEVC	MR Brain (12 bit)	[60.3 - 63.8]	[0.78 - 0.92]	29 - 35 (Intra), 29 - 33 (Inter)	-	-
Zerva *et al.* (2020)[25]	Lossy/ 3D-WDR-MCDP	MR Brain	[50.6 - 52.3]	[0.68 - 0.78]	16	-	-
Guarda *et al.* (2017)[19]	Lossless/ HEVC	2 MR images	-	-	2.8 (0.1), [2.68 - 3.66]	-	-
Pole and Shriam (2018)[58]	Lossy/ HEVC	MR video images of the brain	-	-	10 - 15	-	-
Maheswari and Raghavan (2020)[17]	Lossless/ Tetrolet transform	MRI and CT	-17.8	-	4.18, [4.12 - 4.24]	7.02	-
This work	ROI lossless/ DLAD-HEVC	151 liver CT images	70.03 (0.85)	0.95 (0.02)	6.45 (1.06)	138.5	21.6

From Table 4 and Figure 8, we can conclude that the compression effect of the proposed method does not statistically significantly affect the image quality as assessed by the radiologists for liver lesion detection and lesion center annotation. Note that the ground truth can be at between two slices while the annotations are on a slice, which may cause apart of the displacements. In general, the median displacements for both radiologists are around 2 mm, which are also smaller than the minimal safety margin of 5 mm in the RFA liver intervention[69,70]. Based on the inter-observer scores, we suppose that the median displacements are dominated by the uncertainty in human performance at this task. The main reason, of course, is the selective diffusion, since it does not degrade the quality of the part of the image containing the lesions in the liver. Whereas the visual appearance of the tissue outside the liver in the diffused images is different compared to typical images, this does not seem to hamper the radiologists in their assessment.

Several limitations remain in our study. First, evaluation of the processing time suggests that a large part of the time used for the compression process is the diffusion processing time. In this study, it requires 34.7 [32.4-36.8] seconds using the CPU to diffuse a 3D CT image of around 90 slices (see Table 2). Yet, according to Kalaiselvi (2018)[71], anisotropic diffusion filters can be sped up by 1-2 orders of magnitude when they are implemented on a modern GPU (such as the NVIDIA QUADRO K5000). Furthermore, Wei et.al. (2018)[59] suggested that HEVC compression implementation on a multicore CPU/GPU can save 99% of the processing time. Thus, with the current computational capabilities of modern GPUs, that the processing time of the compression process using DLAD method can be reduced significantly with a hardware-optimized implementation. Secondly, we only demonstrate the compression framework for the purpose of RFA liver intervention using 3D CT abdominal images. However, several recent studies on multi-organ segmentations using CNNs[72,73] have showed that regions of others organs such as the kidneys and spleen can be extracted from the 3D medical images within one minute with high accuracy. In practice, the teleradiologist may not aim to see several organs at once. Thus, the teleradiologist may manually interact with the images to choose the organ of interest; this can then be used to guide the DLAD method to diffuse the images while preserving the organ of interest. Furthermore, we suggest that after the first compressed image is sent, further studies may subsequently transfer the subtraction image and then combine it with the diffused image to fully restore the original image. In order to reduce the delayed time at the receiver, Zerva et al.[25] suggested that progressive transmission of compressed images can be applied. In our proposed framework, a part of the compressed 3D images can be progressively transmitted while the compression process is applied on the remanding part of the images. Thirdly, the HEVC-visually lossless implementation we used in this study only supports a series of 2D images. Nevertheless, we expect HEVC-based compression methods for 3D image compression, using inter-slice information, may further improve CR score at the expense of greater computational resource requirements.

Recently, the Covid-19 pandemic has been first reported in Wuhan in China and spread out to 215 countries around the world within only a few months. The pandemic has become a global threat with at least 40 million infected cases and 1 million deaths[74], causing the lockdowns and the social distancing in many countries around the world. In such a situation, telemedicine in general and teleradiology in particular are a potential solution for clinical diagnosis and treatment. Although the application of the teleradiology still faces many challenges, such as safeguarding privacy and security, we believe that along with the development of telecommunications technology, medical image compression approaches may have a significant contribution on accelerating the use of teleradiology, especially in less well connected areas.

V. CONCLUSIONS

In conclusion, we introduced a framework for teleintervention using 3D medical images. The framework is based on the proposed image processing method, DLAD, which uses a CNN network for region of interest selection and an anisotropic diffusion filter to reduce the entropy of the image without affecting image quality in the region of the organ of interest. DLAD was further combined with a lossless compression method to compress the image. We showed that the method can obtain compression ratios up to 6.45, which is 36% better than compressing without DLAD, while the means of $PSNR$ and $SSIM$ are 70 dB and 0.95, respectively. In addition, we demonstrated that, for liver cancer CT images, images processed in this way do not degrade the detection and localization abilities of radiologists using these images. These results indicated that the compression framework can be used to effectively compress 3D medical images while preserving the quality required for the clinical use. The method thus has a high potential to be implemented in teleradiology applications.

ACKNOWLEDGMENTS

This research is funded by Vietnam National Foundation for Science and Technology Development (NAFOSTED) under grant number 102.01-2018.316. We would like to thank NVIDIA Company for the GPU hardware aid and Mayo Clinic for the CT images. We also would like to thank Mr. Le Quoc Anh for his technical support in this project.

CONFLICT OF INTEREST

The authors have no conflicts to disclose.

ETHICAL STATEMENT

The data from Erasmus Medical Center was obtained under a waiver by the Medical Ethics Committee of the Erasmus MC, University Medical Center Rotterdam. The local medical research ethics committee decided that the Medical Research Involving Human Subjects Act does not apply to this study. The data from the LiTS challenge and Mayo Clinic is publicly available for research, agreed by the local medical research ethics committees.

REFERENCES

[1] S. Srivastava, M. Pant, A. Abraham, and N. Agrawal, The Technological Growth in eHealth Services, 2015, ISSN: 1748-670X Pages: e894171 Publisher: Hindawi Volume: 2015.

[2] A. B. Rosenkrantz, T. N. Hanna, S. D. Steenburg, M. J. Tarrant, R. S. Pyatt, and E. B. Friedberg, The Current State of Teleradiology Across the United States: A National Survey of Radiologists' Habits, Attitudes, and Perceptions on Teleradiology Practice, Journal of the American College of Radiology: JACR **16**, 1677–1687 (2019).

[3] E. R. Ranschaert and F. H. B. Binkhuysen, European Teleradiology now and in the future: results of an online survey, Insights into Imaging **4**, 93–102 (2013).

[4] European Society of Radiology (ESR), ESR teleradiology survey: results, Insights into Imaging **7**, 463–479 (2016).

[5] S. Andronikou, Pediatric teleradiology in low-income settings and the areas for future research in teleradiology, Frontiers in Public Health **2**, 125 (2014).

[6] Hanoi Medical University Hospital - HMU Hospital - YouTube, Accessed: 2020-09-24.

[7] SingLIVE 2020: Scaling Greater Heights - SingHealth, Accessed: 2020-09-24.

[8] J. A. Kaufman and M. J. Lee, *Vascular and Interventional Radiology: The Requisites E-Book*, Elsevier Health Sciences, 2013.

[9] N. Britton, M. A. Miller, S. Safadi, A. Siegel, A. R. Levine, and M. T. McCurdy, Tele-Ultrasound in Resource-Limited Settings: A Systematic Review, Frontiers in Public Health **7**, 244 (2019).

[10] M. R. Meijerink, P. van den Tol, A. A. J. M. van Tilborg, J. H. T. M. van Waesberghe, S. Meijer, and C. van Kuijk, Radiofrequency ablation of large size liver tumours using novel plan-parallel expandable bipolar electrodes: initial clinical experience, European Journal of Radiology **77**, 167–171 (2011).

[11] A. Ahad, M. Tahir, and K.-L. A. Yau, 5G-Based Smart Healthcare Network: Architecture, Taxonomy, Challenges and Future Research Directions, IEEE Access **7**, 100747–100762 (2019), Conference Name: IEEE Access.

[12] T. Lammle, *CompTIA Network+ Study Guide: Exam N10-007*, Comptia Network + Study Guide Authorized Courseware, Sybex, 4 edition, 2018.

[13] S. Kumar and E. Krupinski, *Teleradiology*, Springer Science & Business Media, 2008.

[14] D. A. Clunie, Lossless compression of grayscale medical images: effectiveness of traditional and state-of-the-art approaches, in *Medical Imaging 2000: PACS Design and Evaluation: Engineering and Clinical Issues*, volume 3980, pages 74–84, International Society for Optics and Photonics, 2000.

[15] J. Jiang and C. Grecos, A low cost design of rate controlled JPEG-LS near lossless image compression, Image and Vision Computing **19**, 153–164 (2001).

[16] S. Parikh, H. Kalva, and V. Adzic, Evaluation of HEVC compression for high bit depth medical images, in *2016 IEEE International Conference on Consumer Electronics (ICCE)*, pages 311–314, 2016, ISSN: 2158-4001.

[17] S. UmaMaheswari and V. SrinivasaRaghavan, Lossless medical image compression algorithm using tetrolet transformation, Journal of Ambient Intelligence and Humanized Computing (2020).

[18] H. Amri, A. Khalfallah, M. Gargouri, N. Nebhani, J.-C. Lapayre, and M.-S. Bouhlel, Medical Image Compression Approach Based on Image Resizing, Digital Watermarking and Lossless Compression, Journal of Signal Processing Systems **87**, 203–214 (2017).

[19] A. F. R. Guarda, J. M. Santos, L. A. da Silva Cruz, P. A. A. Assunção, N. M. M. Rodrigues, and S. M. M. de Faria, A method to improve HEVC lossless coding of volumetric medical images, Signal Processing: Image Communication **59**, 96–104 (2017).

[20] L. F. R. Lucas, N. M. M. Rodrigues, L. A. da Silva Cruz, and S. M. M. de Faria, Lossless Compression of Medical Images Using 3-D Predictors, IEEE Transactions on Medical Imaging **36**, 2250–2260 (2017), Conference Name: IEEE Transactions on Medical Imaging.

[21] B. Hulsken, Fast Compression Method for Medical Images on the Web, arXiv:2005.08713 [eess] (2020), arXiv: 2005.08713.

[22] A. Marcelo, P. Fontelo, M. Farolan, and H. Cualing, Effect of image compression on telepathology. A randomized clinical trial, Archives of Pathology & Laboratory Medicine **124**, 1653–1656 (2000).

[23] S. S. Parikh, D. Ruiz, H. Kalva, G. Fernández-Escribano, and V. Adzic, High Bit-Depth Medical Image Compression With HEVC, IEEE Journal of Biomedical and Health Informatics **22**, 552–560 (2018), Conference Name: IEEE Journal of Biomedical and Health Informatics.

[24] U. Sharma, M. Sood, and E. Puthooran, A Block Adaptive Near-Lossless Compression Algorithm for Medical Image Sequences and Diagnostic Quality Assessment, Journal of Digital Imaging **33**, 516–530 (2020).

[25] M. C. Zerva, M. Vrigkas, L. P. Kondi, and C. Nikou, Improving 3D Medical Image Compression Efficiency Using Spatiotemporal Coherence, Electronic Imaging **2020**, 63–1–63–6 (2020).

[26] R. K. Senapati, P. M. K. Prasad, G. Swain, and T. N. Shankar, Volumetric medical image compression using 3D listless embedded block partitioning, SpringerPlus **5**, 2100 (2016).

[27] I. Chaabouni, W. Fourati, and M. S. Bouhlel, Using ROI with ISOM compression to medical image, International Journal of Computational Vision and Robotics **6**, 65 (2016).

[28] P. Sreenivasulu and S. Varadharajan, Algorithmic Analysis on Medical Image Compression Using Improved Rider Optimization Algorithm, in *Innovations in Computer Science and Engineering: Proceedings of 7th ICICSE*, edited by H. S. Saini, R. Sayal, R. Buyya, and G. Aliseri, Lecture Notes in Networks and Systems, pages 267–274, Springer, Singapore, 2020.

[29] T. Heimann et al., Comparison and evaluation of methods for liver segmentation from CT datasets, IEEE transactions on medical imaging **28**, 1251–1265 (2009).

[30] G. Litjens, T. Kooi, B. E. Bejnordi, A. A. A. Setio, F. Ciompi, M. Ghafoorian, J. A. Van Der Laak, B. Van Ginneken, and C. I. Sánchez, A survey on deep learning in medical image analysis, Medical image analysis **42**, 60–88 (2017).

[31] M. Ahmadi, A. Emami, M. Hajabdollahi, S. M. R. Soroushmehr, N. Karimi, S. Samavi, and K. Najarian, Lossless Compression of Angiogram Foreground with Visual Quality Preservation of Background, arXiv:1802.07769 [cs] (2018), arXiv: 1802.07769.

[32] J. P. Ko, H. Rusinek, D. P. Naidich, G. McGuinness, A. N. Rubinowitz, B. S. Leitman, and J. M. Martino, Wavelet Compression of Low-Dose Chest CT Data: Effect on Lung Nodule Detection, Radiology **228**, 70–75 (2003), Publisher: Radiological Society of North America.

[33] M. Moorthi and R. Amutha, A near Lossless compression method for medical images, in *IEEE-International Conference On Advances In Engineering, Science And Management (ICAESM -2012)*, pages 39–44, 2012.

[34] V. K. BAIRAGI and A. M. SAPKAL, ROI-based DICOM image compression for telemedicine, Sadhana **38**, 123–131 (2013).

[35] P. E. Sophia and J. Anitha, Contextual Medical Image Compression using Normalized Wavelet-Transform Coefficients and Prediction, IETE Journal of Research **63**, 671–683 (2017), Publisher: Taylor & Francis _eprint: https://doi.org/10.1080/03772063.2017.1309998.

[36] M. Kaur and V. Wasson, ROI Based Medical Image Compression for Telemedicine Application, Procedia Computer Science **70**, 579–585 (2015).

[37] S. N. Kumar, A. Lenin Fred, and P. Sebastin Varghese, Compression of CT Images using Contextual Vector Quantization with Simulated Annealing for Telemedicine Application, Journal of Medical Systems **42**, 218 (2018).

[38] C. E. Shannon, A mathematical theory of communication, The Bell System Technical Journal **27**, 379–423 (1948), Conference Name: The Bell System Technical Journal.

[39] M. A. Chehab, W. Brinjikji, A. Copelan, and A. M. Venkatesan, Navigational Tools for Interventional Radiology and Interventional Oncology Applications, Seminars in Interventional Radiology **32**, 416–427 (2015), Publisher: Thieme Medical Publishers.

[40] J. Dong, W. Li, Q. Zeng, S. Li, X. Gong, L. Shen, S. Mao, A. Dong, and P. Wu, CT-Guided Percutaneous Step-by-Step Radiofrequency Ablation for the Treatment of Carcinoma in the Caudate Lobe, Medicine **94**, e1594 (2015).

[41] H. M. Luu, *Image Analysis for Guidance in Minimally Invasive Liver Interventions*, 2017, Number: 369.

[42] P. F. Christ, F. Ettlinger, F. Grün, M. E. A. Elshaera, J. Lipkova, S. Schlecht, F. Ahmaddy, S. Tatavarty, M. Bickel, P. Bilic, M. Rempfler, F. Hofmann, M. D. Anastasi, S.-A. Ahmadi, G. Kaissis, J. Holch, W. Sommer, R. Braren, V. Heinemann, and B. Menze, Automatic Liver and Tumor Segmentation of CT and MRI Volumes using Cascaded Fully Convolutional Neural Networks, arXiv:1702.05970 [cs] (2017), arXiv: 1702.05970.

[43] H. H. Son, P. C. Phuong, T. v. Walsum, and L. M. Ha, Liver Segmentation on a Variety of Computed Tomography (CT) Images Based on Convolutional Neural Networks Combined with Connected Components, VNU Journal of Science: Computer Science and Communication Engineering **36** (2020), Number: 1.

[44] P. Perona, T. Shiota, and J. Malik, Anisotropic Diffusion, in *Geometry-Driven Diffusion in Computer Vision*, edited by B. M. ter Haar Romeny, Computational Imaging and Vision, pages 73–92, Springer Netherlands, Dordrecht, 1994.

[45] Z. B. Tariq, N. Arshad, and M. Nabeel, Enhanced LZMA and BZIP2 for improved energy data compression, in *2015 International Conference on Smart Cities and Green ICT Systems (SMARTGREENS)*, pages 1–8, 2015.

[46] L. Prangnell, Visually lossless coding in HEVC: A high bit depth and 4: 4: 4 capable JND-based perceptual quantisation technique for HEVC, Signal Processing: Image Communication **63**, 125–140 (2018).

[47] O. Ronneberger, P. Fischer, and T. Brox, U-Net: Convolutional Networks for Biomedical Image Segmentation, arXiv:1505.04597 [cs] (2015), arXiv: 1505.04597.

[48] H. S. Hoang, C. Phuong Pham, D. Franklin, T. van Walsum, and M. Ha Luu, An Evaluation of CNN-based Liver Segmentation Methods using Multi-types of CT Abdominal Images from Multiple Medical Centers, in *2019 19th International Symposium on Communications and Information Technologies (ISCIT)*, pages 20–25, 2019, ISSN: 2643-6175.

[49] T. M. Cover, *Elements of information theory*, John Wiley & Sons, 1999.

[50] D.-Y. Tsai, Y. Lee, and E. Matsuyama, Information Entropy Measure for Evaluation of Image Quality, Journal of Digital Imaging **21**, 338–347 (2008).

[51] A. Said and W. A. Pearlman, A new, fast, and efficient image codec based on set partitioning in hierarchical trees, IEEE Transactions on Circuits and Systems for Video Technology **6**, 243–250 (1996), Conference Name: IEEE Transactions on Circuits and Systems for Video Technology.

[52] M. Burrows and D. J. Wheeler, A block-sorting lossless data compression algorithm, Technical report, 1994.

[53] D. A. Huffman, A Method for the Construction of Minimum-Redundancy Codes, Proceedings of the IRE **40**, 1098–1101 (1952), Conference Name: Proceedings of the IRE.

[54] P. Ferragina and G. Manzini, Indexing compressed text, Journal of the ACM **52**, 552–581 (2005).

[55] R. A. Patel, Y. Zhang, J. Mak, A. Davidson, and J. D. Owens, Parallel lossless data compression on the GPU, in *2012 Innovative Parallel Computing (InPar)*, pages 1–9, 2012.

[56] G. J. Sullivan, J.-R. Ohm, W.-J. Han, and T. Wiegand, Overview of the High Efficiency Video Coding (HEVC) Standard, IEEE Transactions on Circuits and Systems for Video Technology **22**, 1649–1668 (2012), Conference Name: IEEE Transactions on Circuits and Systems for Video Technology.

[57] V. Sanchez and J. Bartrina-Rapesta, Lossless compression of medical images based on HEVC intra coding, in *2014 IEEE International Conference on Acoustics, Speech and Signal Processing (ICASSP)*, pages 6622–6626, 2014, ISSN: 2379-190X.

[58] A. Pole and R. Shriram, 3-D Medical Image Compression by Using HEVC, in *2018 Fourth International Conference on Computing Communication Control and Automation (ICCUBEA)*, pages 1–5, 2018.

[59] W. Xiao, B. Li, J. Xu, G. Shi, and F. Wu, HEVC Encoding Optimization Using Multicore CPUs and GPUs, IEEE Transactions on Circuits and Systems for Video Technology **25**, 1830–1843 (2015), Conference Name: IEEE Transactions on Circuits and Systems for Video Technology.

[60] H. M. Luu, C. Klink, W. Niessen, A. Moelker, and T. v. Walsum, Non-Rigid Registration of Liver CT Images for CT-Guided Ablation of Liver Tumors, PLOS ONE **11**, e0161600 (2016), Publisher: Public Library of Science.

[61] Z. Wang, A. Bovik, H. Sheikh, and E. Simoncelli, Image quality assessment: from error visibility to structural similarity, IEEE Transactions on Image Processing **13**, 600–612 (2004), Conference Name: IEEE Transactions on Image Processing.

[62] G. P. Renieblas, A. T. Nogués, A. M. González, N. Gómez-Leon, and E. G. Del Castillo, Structural similarity index family for image quality assessment in radiological images, Journal of Medical Imaging (Bellingham, Wash.) **4**, 035501 (2017).

[63] P. Andersson, J. Nilsson, T. Akenine-Möller, M. Oskarsson, K. Åström, and M. D. Fairchild, FLIP: A Difference Evaluator for Alternating Images, Proceedings of the ACM on Computer Graphics and Interactive Techniques **3**, 15:1–15:23 (2020).

[64] C. H. McCollough, A. C. Bartley, R. E. Carter, B. Chen, T. A. Drees, P. Edwards, D. R. Holmes, A. E. Huang, F. Khan, S. Leng, K. L. McMillan, G. J. Michalak, K. M. Nunez, L. Yu,

and J. G. Fletcher, Low-dose CT for the detection and classification of metastatic liver lesions: Results of the 2016 Low Dose CT Grand Challenge, Medical Physics **44**, e339–e352 (2017), _eprint: https://aapm.onlinelibrary.wiley.com/doi/pdf/10.1002/mp.12345.

[65] P. Bilic et al., The Liver Tumor Segmentation Benchmark (LiTS), arXiv:1901.04056 [cs] (2019), arXiv: 1901.04056 version: 1.

[66] J. R. Flynn, S. Ward, J. Abich, and D. Poole, Image Quality Assessment Using the SSIM and the Just Noticeable Difference Paradigm, in *Engineering Psychology and Cognitive Ergonomics. Understanding Human Cognition*, edited by D. Harris, Lecture Notes in Computer Science, pages 23–30, Berlin, Heidelberg, 2013, Springer.

[67] J. G. Fletcher, J. L. Fidler, S. K. Venkatesh, D. M. Hough, N. Takahashi, L. Yu, M. Johnson, S. Leng, D. R. Holmes, R. Carter, and C. H. McCollough, Observer Performance with Varying Radiation Dose and Reconstruction Methods for Detection of Hepatic Metastases, Radiology **289**, 455–464 (2018), Publisher: Radiological Society of North America.

[68] B. Bross, J. Chen, and S. Liu, Versatile video coding (Draft 5), JVET-K1001 (2018).

[69] K. W. Kim, J. M. Lee, E. Klotz, S. J. Kim, S. H. Kim, J. Y. Kim, J. K. Han, and B. I. Choi, Safety margin assessment after radiofrequency ablation of the liver using registration of preprocedure and postprocedure CT images, American Journal of Roentgenology **196**, W565–W572 (2011).

[70] Y. Minami and M. Kudo, Radiofrequency ablation of hepatocellular carcinoma: a literature review, International journal of hepatology **2011** (2011).

[71] T. Kalaiselvi, P. Sriramakrishnan, and K. Somasundaram, Performance of Medical Image Processing Algorithms Implemented in CUDA running on GPU based Machine, International Journal of Intelligent Systems and Applications **10**, 58 (2018).

[72] E. Gibson, F. Giganti, Y. Hu, E. Bonmati, S. Bandula, K. Gurusamy, B. Davidson, S. P. Pereira, M. J. Clarkson, and D. C. Barratt, Automatic Multi-Organ Segmentation on Abdominal CT With Dense V-Networks, IEEE Transactions on Medical Imaging **37**, 1822–1834 (2018), Conference Name: IEEE Transactions on Medical Imaging.

[73] Y. Fu, Y. Lei, T. Wang, S. Tian, P. Patel, A. B. Jani, W. J. Curran, T. Liu, and X. Yang, Pelvic multi-organ segmentation on cone-beam CT for prostate adaptive radiotherapy, Medical Physics **47**, 3415–3422 (2020).

[74] WHO Coronavirus Disease (COVID-19) Dashboard, Accessed: 2020-10-19.